Pertanika J. Sci. & Technol. 31 (1): 577 - 594 (2023)

PERTANIKA JOURNALS

SCIENCE & TECHNOLOGY

Journal homepage: http://www.pertanika.upm.edu.my/

Brain Tumour Region Extraction Using Novel Self-Organising Map-Based KFCM Algorithm

Peddamallu Gangadhara Reddy[1]*, Tirumala Ramashri[1] and Kayam Lokesh Krishna[2]

[1]Department of ECE, Sri Venkateswara University College of Engineering, S.V. University, Tirupati, A.P., India
[2]Department of ECE, S.V. College of Engineering, Tirupati, A.P., India

ABSTRACT

Medical professionals need help finding tumours in the ground truth image of the brain because the tumours' location, contrast, intensity, size, and shape vary between images because of different acquisition methods, modalities, and the patient's age. The medical examiner has difficulty manually separating a tumour from other parts of a Magnetic Resonance Imaging (MRI) image. Many semi- and fully automated brain tumour detection systems have been written about in the literature, and they keep improving. The segmentation literature has seen several transformations throughout the years. An in-depth examination of these methods will be the focus of this investigation. We look at the most recent soft computing technologies used in MRI brain analysis through several review papers. This study looks at Self-Organising maps (SOM) with K-means and the kernel Fuzzy c-means (KFCM) method for segmenting them. The suggested SOM networks were first compared to K-means analysis in an experiment based on datasets with well-known cluster solutions. Later, the SOM is combined with KFCM, reducing time complexity and producing more accurate results than other methods. Experiments show that skewed data improves networks' performance with more SOMs. Finally, performance measures in real-time datasets are analysed using machine learning approaches. The results show that the proposed algorithm has good sensitivity and better accuracy than k-means and other state-of-art methods.

ARTICLE INFO

Article history:
Received: 30 March 2022
Accepted: 28 June 2022
Published: 27 December 2022

DOI: https://doi.org/10.47836/pjst.31.1.33

E-mail addresses:
gangadharareddy.p@gmail.com (Peddamallu Gangadhara Reddy)
rama.jaypee@gmail.com (Tirumala Ramashri)
kayamlokesh78@gmail.com (Kayam Lokesh Krishna)
* Corresponding author

Keywords: Brain tumour segmentation, feature extraction, kernel FCM, K-means, medical imaging, self-organising map

INTRODUCTION

MRI utilises radio waves and a magnetic field to create precise pictures of the brain and brain stem. It is a painless and safe

ISSN: 0128-7680
e-ISSN: 2231-8526

© Universiti Putra Malaysia Press

procedure. Because it does not utilise radiation, magnetic resonance imaging differs from computed tomography. An MRI scan may detect cysts, tumours, haemorrhages, oedema, and structural brain abnormalities. A brain MRI may help patients to find the cause of their symptoms, like persistent headaches, dizziness, paralysis, or seizures. Additionally, it can diagnose chronic nervous system illnesses such as multiple sclerosis. At times, an MRI may provide a more detailed image of the brain than an ultrasound Computed Tomography (CT) scan or X-ray (Zhang & Sejdić, 2019).

The most efficient segmentation approach relied on a grey-level information process in which organs with comparable intensities make it challenging to determine the tumour's location. Kohonen developed an unsupervised SOM neural network using a competitive learning method with an automated topological mapping procedure that reduces the number of dimensions to one or two (Şişik & Eser, 2020). Thus far, the picture segmentation method provided by the SOM neural network has been more attractive. On the other hand, an automated SOM neural network classification method generates feature vectors that help with the colour picture segmentation process (Kumar et al., 2019).

When used in image segmentation, SOM neural networks used two-stage classification algorithms that employed a predetermined noise reduction (Garcia-Lamont et al., 2018). The automated ideal cluster centre was obtained using a fuzzy clustering algorithm with a SOM neural network. An unsupervised segmentation technique supports a trained network that performs dimension reduction. SOM segmentation using fuzzy clustering is compared to an Efficient Graph (EG)-based segmentation approach in the centre initialisation procedure (Kumar et al., 2018 & Sandhya et al., 2019). Halder's research team suggested a SOM neural network with modal analysis and mutational aggregation for automatic classification. However, it is not self-contained and requires a mapping technique and dimension reduction (Garcia-Lamont et al., 2018). Segmentation is more efficient using the 2D discrete wavelet transform with the Moving Average SOM (MASOM) method, as it ensures the least human involvement in modifying the variables that initiate the segmentation process. This technique combines clustering with a self-organising map to achieve successful MRI image segmentation, as shown in Figure 1. This method has the main drawback of using additional computing time during the segmentation procedure.

Tumours in the brain are made up of aberrant cells that develop quickly and that the body cannot manage. Brain tumours continue to develop at an accelerated rate, and their appearance determines whether they are benign or malignant. The skull is a static bone structure. As a result, the skull cannot grow, and the tumour begins to push on the brain once it has formed. Primary brain cancers occur when tumours originate in the brain.

On the other hand, cancer develops in other body areas and spreads to the brain (Anaraki et al., 2019), and it is considered secondary or metastatic. Tumours in the brain may spread at varying rates. The tumour's location determines the rate at which it grows. The tumour's

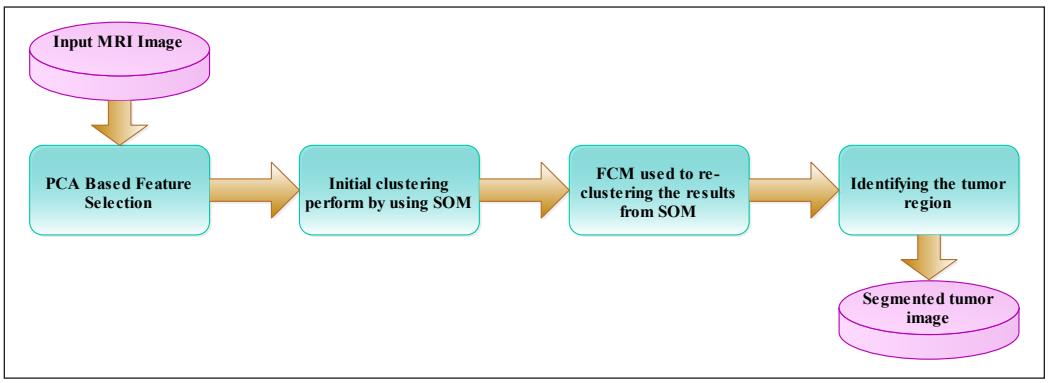

Figure 1. The basic segmentation flow for SOM based clustering algorithm

location is also critical in terms of neurological impairment. Simultaneously, tumour therapy depends on the size, location, and kind of tumour (Mohan & Subashini, 2019 & Tarhini & Shbib, 2020). The research attempted to bring some benchmark segmentation methods in medical image analysis, which have been thoroughly studied. To segment medical images used, the fuzzy C-means method, a new FCM method that heavily relies on the neighbourhood means to determine the goal function. The enhanced FCM algorithm revealed non-local information in the neighbour function (Song et al., 2022). The modified genetic algorithm crossover and mutation process are used to process the input picture by the algorithm, which is used to make the final segmentation result. Particle Swarm Optimization (PSO)-FCM and a region-growing algorithm are used to get more precise tumour detection at the cost of longer processing times. A modified fuzzy K-means method based on bacteria foraging optimisation takes less time to provide segmentation results (Vishnuvarthanan et al., 2017 & Sandhya et al., 2020). The semi-supervised method is the moving average SOM algorithm to get excellent segmentation results with little human involvement. A SOM neural network utilising dynamic spanning trees needs a longer learning time to give excellent segmentation results. For MR brain imaging, the SOM-based fuzzy K means (FKM) method aids in detecting tumour heterogeneity (Mohan & Subashini, 2018). The author recommends using the Brain Extraction Tool (BET) when preparing medical pictures that heavily rely on human interaction. The SOM-based Learning Vector Quantization (LVQ) method aids in analysing MRI brain images using the method to obtain the image segmentation results may be generated quickly and with little input from the user (Vijh et al., 2020 & Ejaz et al., 2020). Helmy and El-Taweel (2016) introduce the pulse-coupled neural network method, which is unquestionably a step forward in supervised clustering. The SOM method uses a modified pulse-coupled neural network to build an automatic cluster centre. On the other hand, the Entropy Gradient Segmentation-Self Organization Map (EGS-SOM) method uses the genetic algorithm to determine the cluster centre's location (Al-Dmour & Al-Ani, 2018). It uses the statistical feature to execute the clustering

operation in a unique SOM-based FCM technique. A novel hybrid segmentation technique to produce performance-oriented segmentation based on Different clustering methods (Ejaz et al., 2020). A comparative analysis of parameters like sensitivity and selectivity resulted in K-means, Gaussian Mixture Model (GMM) and FCM algorithms (Baid et al., 2017). An effective brain tumour classification and segmentation for identifying the tumour and non-tumour cells in the brain (Krishnakumar & Manivannan, 2021).

A brain tumour segmentation approach is proposed based on an extreme learning machine and significantly fast and robust fuzzy C-means clustering algorithms (BTS-ELM-FRFCM) running on Raspberry Pi (PRI) hardware (Şişik & Eser, 2020). The algorithm combines Region of Interest (ROI), Region Growing and Morphological Operation, and FCM (Sheela & Suganthi, 2020). Computer-aided robotic research technology is incorporated to effectively diagnose the brain tumour at the initial stage with improved accuracy (Balamurugan et al., 2021). The Neural Network architecture does leaf image clustering, self-organising map (SOM), and K-Means algorithm for generating the sub-images by clustering the pixels based on the colours (Kumar et al., 2019), the basic features such as entropy, mean, and standard deviation are extracted from each sub-images. A novel weighted spatial kernel FCM clustering for segmenting the region of interest in the medical image (Kumar et al., 2018).

An automatic brain tumour MRI Data segmentation framework proposed a combined segmentation model based on VNet, integrating the SE and AG modules. By using volume input, three-dimensional convolution is used to process MRI images, get excellent segmentation results, and have the potential clinical application (Guan et al., 2021). A deep multi-task learning framework utilises a decoder for v-net for better segmentation which works on multiple datasets (Huang et al., 2021). A novel network structure with Multi-Encoder with different modalities greatly improves the segmentation performance. Network (ME-Net), a new architecture composed of four encoders performing on the Multimodal Brain Tumour Segmentation Challenge (BraTS) 2020 dataset and compared it with the results of other teams participating in the challenge. The results show that our model has a promising performance for brain tumour segmentation (Zhang et al., 2021). A fully automated method of detection and segmentation of the abnormal tissue associated with a brain tumour (tumour core and oedema) from Fluid Attenuated Inversion Recovery (FLAIR) Magnetic Resonance Imaging (MRI). Results demonstrate the high detection and segmentation performance of the proposed method using ERT classifier, which is a faster and more reproducible method of brain tumour detection and delineation to aid patient management (Soltaninejad et al., 2018).

GAN is a neural network that can translate an image from one domain to another using unpaired data. It alleviates the problem posed by a lack of paired datasets since there is a vast amount of unpaired image data. On the other hand, the main advantage of using a

SOM is that the data is easily interpreted and understood. Furthermore, the reduction of dimensionality and grid clustering makes it easy to observe similarities in the data.

The Supervoxels method demonstrates promising results in the segmentation of brain tumours. Multimodal MRI images increase the segmentation accuracy, which gives a faster and more reproducible method of brain tumour detection (Soltaninejad et al., 2018).

Any researcher interested in classification should not use an unsupervised learning scheme like K-means or SOM because data clusters may not match class distributions. Instead, learning vector quantisers (LVQ) or SVMs should be applied. If applying any unsupervised learning for those problems with a post-labelling, the accuracy might not be the best because the unsupervised learning goal differs from classification.

METHODS

MRI brain tumour images were segmented using algorithms like K-Means, Fuzzy C-Means, Kernal Fuzzy C-Means, and Self-Organising Map techniques. These strategies will be briefly explored in the following sections (Mohan & Subashini, 2018).

K-Means Clustering

Samples are divided into k clusters with the closest cluster centroid using K-Means clustering (Osman & Alzahrani, 2018) as a vector quantisation technique. Assume that the *n* input vectors x_1, x_2,...,x_n are real-valued and d-dimensional. Then, C_1, C_2,..., C_k represent the k clusters in which these sample vectors have been divided. As stated in Equation 1, this method minimises the cluster sum. In this case, let μ_i represent the average of the C_i samples.

$$\arg \min_{c} \sum_{i=1}^{k} \sum_{x \in C_i} ||x - \mu_i||^2 \quad [1]$$

To get the solution for x in Equation 1, we must solve for x in Equation 2.

$$\arg \min_{c} \sum_{i=1}^{k} \frac{1}{2|C_i|} \sum_{x,y \in C_i} ||x - y||^2 \quad [2]$$

When using the conventional K-Means technique, accuracy improved with the iterative refinement method (Asliyan & Atbakan, 2020). The K-means algorithm considers two stages, like initial and updated stages. In other words, we will say that the initial set of K-means is made up of $m_1(1)$,$m_2(1)$,..., $m_k(1)$.

The first step is to compute the distances between the samples and the means using the least squared Euclidean distance and then place each sample in the cluster to which it is closest. In this case, sample x is placed precisely in cluster C(t), the number of iterations is t, and clusters are i, respectively, as shown in Equation 3.

$$C_i(t) = \left\{x: \left||x - m_i(t)|\right|^2 \leq \left||x - m_j(t)\right|\right|^2, 1 \leq j \leq k\right\} \quad [3]$$

In the update step, we obtain the means (m_i) of all clusters' samples according to Equation 4.

$$m_i(t+1) = \frac{1}{C_i(t)} \sum_{x_j \in C_i(t)} x_j \quad [4]$$

A standard K-means algorithm consists of the steps shown below:

(1) Set the number of clusters to k and create them randomly or generate cluster centres (k).
(2) Use Euclidean distance to define every location here to the cluster centre that is closest to it.
(3) Use the new data to figure out which cluster centres should be added.
(4) Repeat procedures (2) and (3) as necessary until the convergence criteria are satisfied.

Fuzzy C-Means Clustering

Fuzzy C-Means is a technique for unsupervised clustering that divides data into k groups (Ren et al., 2019; Sheela & Suganthi, 2020). Dunn invented this technique in 1973, and Bezdek refined it in 1981, intending to minimise an objective function as stated in Equation 5.

$$\arg \min_c \sum_{i=1}^{n} \sum_{j=1}^{c} \mu_{ij}^m \left|x_i - c_j\right|^2 \quad [5]$$

where m is a positive integer larger than 1, x_i is the i^{th} dimension of d-dimensional measured data, c_j is the cluster's d-dimension centre, and μ_{ij} is the degree of membership of x_i in cluster j. Membership μ_{ij} and cluster centres c_j are changed in each iteration, as illustrated in Equations 6 and 7.

$$\mu_{ij} = \frac{1}{\sum_{k=1}^{c} \left\{\frac{\left\|x_i - c_j\right\|}{\left\|x_i - c_k\right\|}\right\}^{(2/m-1)}} \quad [6]$$

$$c_j = \frac{\sum_{i=1}^{n} \mu_{ij}^m \, x_i}{\sum_{i=1}^{n} \mu_{ij}^m} \quad [7]$$

If xy=0, the iteration is complete. δ is a real number between 0 and 1, and there are t iterations.

Self-Organising Map (SOM)

SOM is an instance of a self-organising map (Şişik & Eser, 2020). It is an unsupervised artificial neural network. Additionally, SOM employs competitive learning and dimension reduction. As shown in Figure 2, it creates a map representing the input space in a low-dimensional manner. In the 1980s, Kohonen invented this technique, and Kohonen Map got its name for this reason.

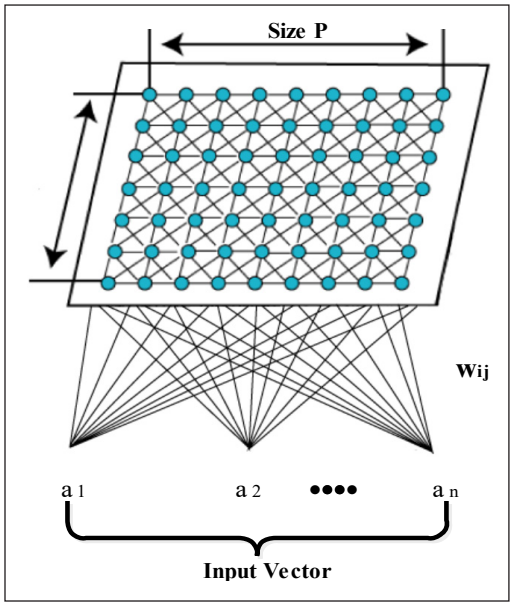

Figure 2. Fundamental architecture for SOM

Proposed SOM-KFCM

Our proposed method trains a SOM neural network on colour picture characteristics with and without a saliency map. All these steps are done to ensure that the output prototype vectors are filtered and aggregated using a k-means-based image segmentation assessment index. The method also has preprocessed and post-processing stages. Figure 3 depicts a comprehensive flowchart of the SOM-KFCM technique. This same flowchart is used for the SOM-Kmeans technique. The main difference here is that KFCM contains a saliency map module, but Kmeans does not have a saliency map.

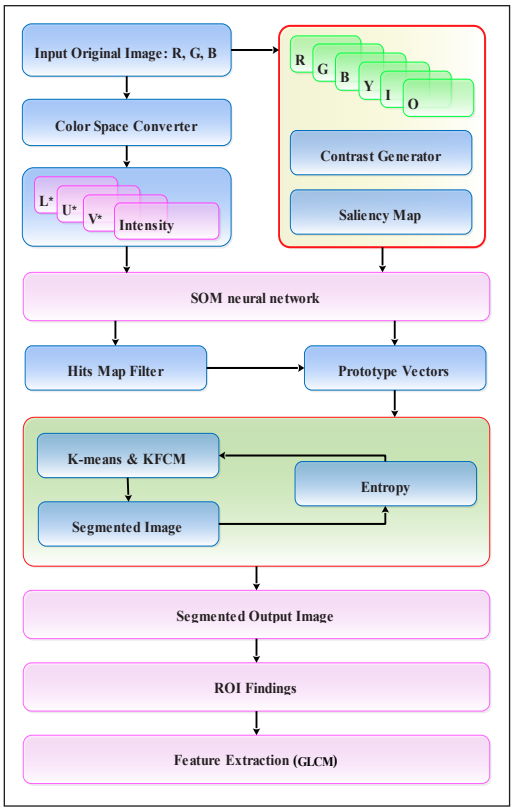

Figure 3. Architecture of SOM-KFCM technique

Self-Organising Map. Unsupervised artificial neural networks like SOM, initially proposed by Kohonen, are extensively utilised (Song et al., 2021). In most cases, the map is a collection of prototype vectors representing node units in a two-dimensional space, although nodes may also be in a single or multiple spaces. For example, a neighbourhood function connects apartments to the apartments next door. Initialisation techniques for prototype

vectors are random and linear, then "folded" in a two-dimensional space. After that, they are trained sequentially or in batches using randomly chosen input samples and then updated based on the neighbours' results. Once trained, the prototype velocities become stable and "unfold" in the two-dimensional space map. It is very uncommon for SOM to include capabilities like seeing a system's topology and the ability to represent many different input patterns (such as those with p samples and m dimensions) using a minimal number of nodes. The nodes map is among SOM's most significant features, representing the input patterns that are topologically close to one other in the output space.

According to Kohonen, a prototype vector w_i = exists for each node i [20-21]. (w_{i1}, w_{i2}, . . . , w_{im}). The similarity rule chooses a winning node, c, for each input sample x. This node is represented by Equation 8.

$$c = \arg\ min_i \{\|x - w_i\|\} \quad [8]$$

in other words, the same thing can be written as in Equation 9

$$\{\|x - w_i\|\} = min_i \{\|x - w_i\|\} \quad [9]$$

where $\|.\|$ denotes the Euclidean distance between two points. Equation 10 updates the weights of the winning node c (prototype vector) and its neighbours' nodes.

$$w_i(t+1) = w_i(t) + h_{ci}(t)[x(t) - w_i(t)] \quad [10]$$

Equation 11 shows the winning node c neighbourhood function $h_{ci,}$ and t is the current training iteration with input sample x(t) utilised. For example, the learning rate α (t) and the neighbourhood function h reduce the iteration time and the distance between each source and destination node.

$$h_{ci}(t) = \alpha(t)(\|r_c - r_i\|, t) \quad [11]$$

where r_i and r_c are the locations of the winning nodes i and c in the topological map, respectively, and α (t) is the learning rate.

This method is efficient even if the model vectors' initial values do not match the data distribution. Because the previous strategy does not include a learning rate parameter, it has no convergence issue, and the asymptotic values of w_i are more stable than the original approach. Generally, a few repeats of this approach are sufficient (Vijh et al., 2020).

Each input sample has a maximum output node. When the input sample "hits" the node, it affects it. The more input samples a node has, the more hits it may return. Nodes in a 2-dimensional SOM map represent the structure of a multidimensional space inside

input feature patterns. SOM groups the nodes to organise the input feature patterns (pixels for an image).

Proposed SOM Algorithm:

1) SOM neurons' weights are set to random values at the start of the simulation.
2) The training data set randomly selects an input vector, x.
3) No distances exist between the input vector and any neurons or units. Therefore, the winning neuron is the one with the shortest distance.
4) When a winning neuron is found, its area is computed.
5) The weights of nearby neurons affected by the winning neuron (including the winning neuron) are shown by Equation 12. In other words, the input vector is becoming closer to the neurons.

$$w_v(t+1) = w_v(t) + \beta(u, v, t)[x - w_v(t)] \quad [12]$$

Step 2 should be repeated as many times as iterations in N.

The current iteration, t, is assumed to be the iteration, v is the neuron index in the map, Wv is the current weight vector of the neuron v, and β(u, v, t) is the neighbourhood function.

Kernel-FCM Clustering Algorithm. The FCM method outperforms the Hard C-Mean (HCM) algorithm in terms of clustering accuracy. By incorporating the kernel approach into clustering, this study may successfully address the drawbacks of the FCM methodology. The Kernel FCM works by nonlinearly mapping the input model space R^s to high-dimensional feature space and then performing FCM clustering in high-dimensional feature space. The Mercer condition is the most extensively used nonlinear transformation. Usually, base kernel functions are polynomial and radial. A feature space is $X = \{x_1, x_2, \ldots \ldots x_n\} \subset R^q$, i.e., dataset R^s is mapped to a feature space R^q, where c, the number of classes to be separated is $2 \leq c \leq N$, and now the goal function is:

$$J_{km}(U, V) = \sum_{i=1}^{c} \sum_{j=1}^{N} \mu_{ij}^m \left\| \psi(x_j) - \psi(v_i) \right\|^2 = \sum_{i=1}^{c} \sum_{j=1}^{N} \mu_{ij}^m \, d_{kij}^2 (x_j - v_i) \quad [13]$$

K=1,2,3….Nand i=1,2,3….c

In Equation 13, m denotes the control index of fuzzy, and μ_{ij} is the membership degree of the j^{th} data pair i. The Euclid distance between R^q and the two vectors x_i and x_j may be expressed using the kernel function K in this chosen Equation 14.

$$d_{Kij} = \left[K(x_i, x_i) - 2K(x_i, x_j) + K(x_j, x_j) \right]^{1/2} \quad [14]$$

When the Lagrange multiplier optimisation technique is used to solve Equations 15 and 16, the resulting objective function is as follows:

$$\mu_{ij} = \frac{\left(1/d_{kij}^2(x_j, v_i)\right)^{1/m-1}}{\sum_{i=1}^{c}\left(1/d_{kij}^2(x_j, v_i)\right)^{1/m-1}} \quad [15]$$

$$v_i = \frac{\left(1/d_{kij}^2(x_j, v_i)\right)^{1/m-1}}{\sum_{i=1}^{N}(\mu_{ij}^m K(x_j, v_i))} \quad [16]$$

The iteration is over when the last partition matrices U and V are found. Furthermore, KFCM can group a lot of different types of data. The only thing it does not give is how the classes work together. When the size of the data set changes a lot, the impact of clustering is not as significant as it could be.

RESULTS AND DISCUSSION

The methodology of the proposed method was described above, and the results are shown in Tables 1 to 4 and Figure 4. Table 1 compares the proposed SOM-based Kmeans and KFCM algorithm's average picture quality parameter values to those of other conventional image segmentation algorithms, which aids in verifying the algorithm's efficiency.

Figure 4a shows the input images used to train the SOM neural network. An 8 x 8 map construction may be used to generate an efficient pixel classification procedure, and this map is provided as input to the KFCM method by the SOM. Consequently, a significant incentive for the re-clustered procedure to achieve the automated cluster centre is categorisation derived from the map structure. Finally, the scanned and segmented images identified the tumour and lesion areas.

SOM-based KFCM algorithm provides excellent segmentation; compared to the suggested SOM-based K-means method, an enlarged cyst tumour in the right hepatic lobe may be easily detected in Figures 4b and 4c. The proposed SOM-based K-means and KFCM method successfully segment the brain, lungs and liver, demonstrating the usefulness of identifying the tumour area. The work in this paper identifies brain tumours only. We mainly consider brain tumour segmentation as it is also suitable for other tumour segmentation, like support for lung and liver segmentation.

The results of the comparison of K-means and the KFCM method are shown in Tables 1, 2 and 3 in terms of simulated, statistical, and quality performance. Glioma and metastatic bronchogenic carcinoma patients' brain tumours are shown in Figures 4b and 4c. The suggested SOM-based KFCM algorithm m's input picture is shown in Figure 4a. The suggested technique clearly distinguished the tumour's precise location and the surrounding grey and white matter.

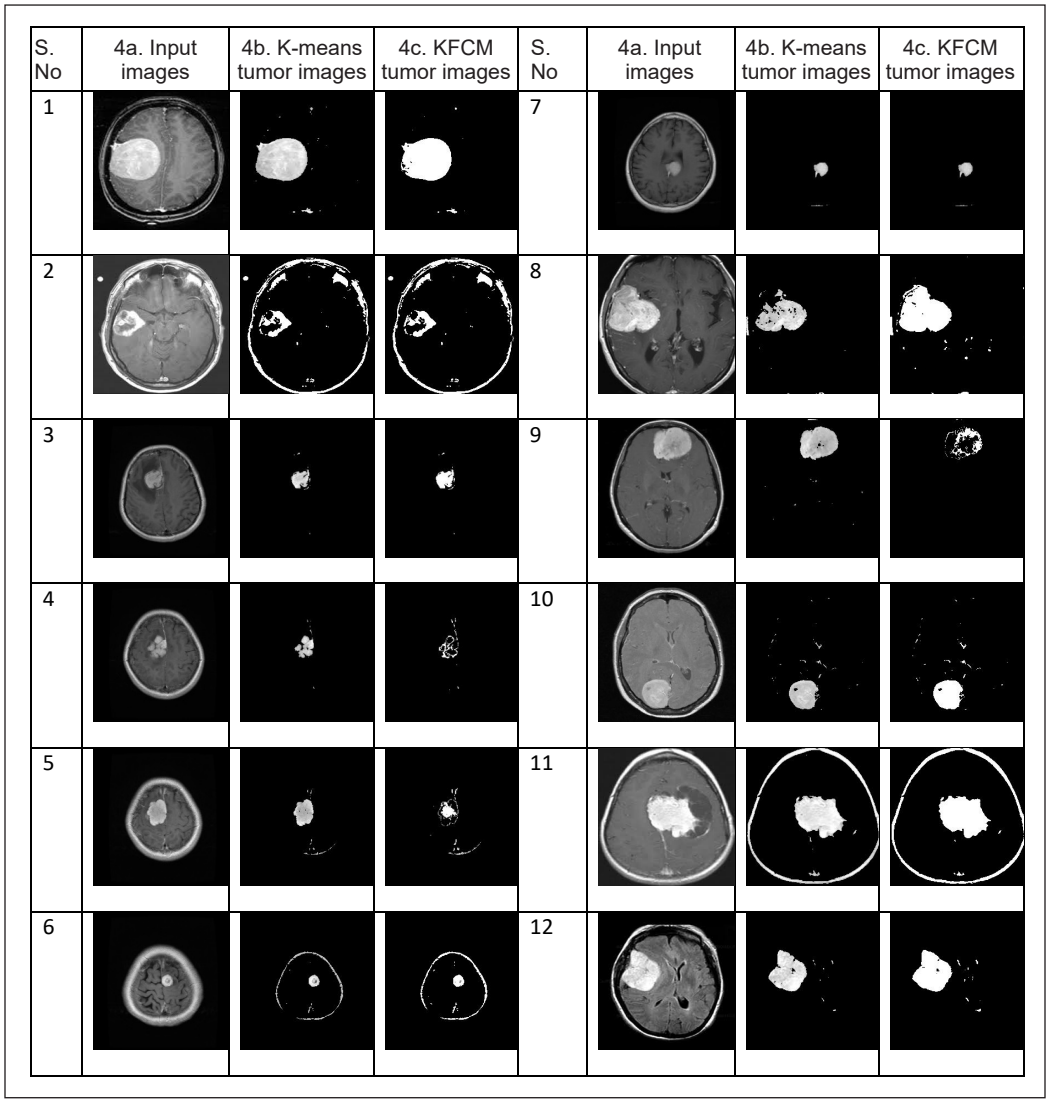

Figure 4. Segmented tumour detection and feature extraction results

A comparison of competing soft computing methods is shown in Tables 1 and 2, where the average values of evaluation parameters are shown. Compared to other conventional algorithms, the suggested SOM-based KFCM method has an average performance value Energy returns the sum of squared elements in the GLCM Range is [0 1], and the Energy is 1 for a constant image.

Table 3 demonstrates that the statistical metrics of Laplacian operators are similar to the ideal values. Measurement of Diagonal Laplacian (LAPD) focus yields somewhat improved results. For example, Mean Square Error (MSE) is a standard and fundamental metric for assessing distortion. There is a difference between the processed picture and

Table 1
Simulated performance analysis

Images	SOM K-means						SOM-KFCM					
	Tumour Area	No. of Pixels	r_cr	r_bpp	n_cr	n_bpp	Tumour Area	No. of Pixels	r_cr	r_bpp	n_cr	n_bpp
Flair_1	0.0968	6050	7.5170	1.0643	7.6107	1.0512	0.0916	5725	8.0265	0.9967	9.2046	0.8691
Flair_2	0.6076	37972	1.6049	4.9848	4.1569	1.9245	0.0884	5528	8.7148	0.9180	4.4307	1.8056
Flair_3	0.0128	803	45.6739	0.1752	9.8022	0.8161	0.0128	803	45.6739	0.1752	9.8022	0.8161
Flair_4	0.0133	831	42.9141	0.1864	10.8713	0.7359	0.0064	402	85.0327	0.0941	13.6461	0.5862
Flair_5	0.0227	1416	26.7776	0.2988	11.2469	0.7113	0.0117	732	51.1658	0.1564	12.9963	0.6156
Flair_6	0.0192	1198	30.7650	0.2600	10.6781	0.7492	0.0210	1315	28.2051	0.2836	13.6580	0.5857
Flair_7	0.0082	515	67.9984	0.1176	10.5662	0.7571	0.0962	6015	10.2275	0.7822	8.6672	0.9230
Flair_8	0.0639	3991	10.9652	0.7296	6.4954	1.2316	0.0938	5865	7.3999	1.0811	5.2069	1.5364
T1_1	0.0519	3246	13.1438	0.6086	7.6676	1.0433	0.0165	1033	43.0286	0.1859	8.8903	0.8999
T1_2	0.0377	2354	18.0548	0.4431	8.3959	0.9528	0.0381	2381	17.8377	0.4485	8.3332	0.9600
T1_3	0.1500	9374	5.1773	1.5452	4.2875	1.8659	0.1416	8849	5.5190	1.4495	5.5427	1.4434
T1_4	0.0539	3366	12.6555	0.6321	8.6480	0.9251	0.0568	3550	11.9148	0.6714	6.6887	1.1961
T1_5	0.0963	6017	7.2026	1.1107	5.3920	1.4837	0.0343	2141	19.1899	0.4169	6.2587	1.2782
T1_6	0.0481	3009	14.3490	0.5575	13.0560	0.6127	0.0491	3070	14.0018	0.5714	13.0751	0.6118
T1_7	0.0177	1105	34.7120	0.2305	8.0915	0.9887	0.0931	5816	9.5582	0.8370	5.5873	1.4318
T1_8	0.0655	4095	10.6422	0.7517	6.5747	1.2168	0.0660	4125	10.5492	0.7583	6.5795	1.2159
T2_1	0.0109	680	58.6157	0.1365	8.4230	0.9498	0.0103	642	63.0110	0.1270	11.4174	0.7007
T2_2	0.0118	740	47.8828	0.1671	11.9410	0.6700	0.0092	573	62.0723	0.1289	16.1496	0.4954
T2_3	0.0104	648	55.3762	0.1445	13.3203	0.6006	0.0103	643	55.8338	0.1433	13.3118	0.6010
T2_4	0.0136	853	41.8088	0.1913	11.1208	0.7194	0.0132	824	43.2631	0.1849	11.1228	0.7192
T2_5	0.0157	979	38.7441	0.2065	12.2619	0.6524	0.0350	2190	18.1288	0.4413	16.6132	0.4815
T2_6	0.1394	8712	6.0914	1.3133	8.4356	0.9484	0.0133	831	44.7580	0.1787	13.4958	0.5928
T2_7	0.0139	871	42.5996	0.1878	10.9917	0.7278	0.0133	831	44.7580	0.1787	13.4958	0.5928
T2_8	0.0178	1110	34.1198	0.2345	10.5680	0.7570	0.0180	1127	33.6039	0.2381	10.5501	0.7583

* cr - compression ratio, bpp - bits per pixel

Table 2
Statistical features analysis

Images	SOM K-means				SOM-KFCM			
	Contrast	Correlation	Energy	Homogeneity	Contrast	Correlation	Energy	Homogeneity
Flair_1	0.19994	0.97675	0.99820	0.99643	0.20309	0.97518	0.82885	0.99637
Flair_2	2.16158	0.90728	0.98204	0.96140	1.37913	0.82609	0.81081	0.97537
Flair_3	0.12595	0.89907	0.97197	0.99775	0.12595	0.89907	0.97197	0.99775
Flair_4	0.13854	0.89267	0.97084	0.99753	0.26292	0.58188	0.98183	0.99531
Flair_5	0.18892	0.91328	0.99170	0.99663	0.34951	0.69311	0.96968	0.99376
Flair_6	0.45026	0.75658	0.98534	0.99196	0.47073	0.76772	0.94913	0.99159
Flair_7	0.05825	0.92756	0.98240	0.99896	0.92257	0.89216	0.80694	0.98353
Flair_8	0.37706	0.93570	0.98727	0.99327	0.38886	0.95340	0.82186	0.99306
T1_1	0.16531	0.96587	0.89778	0.99705	0.42350	0.73520	0.95879	0.99244
T1_2	0.25819	0.98759	0.92199	0.99539	0.26606	0.92620	0.92103	0.99525
T1_3	1.00601	0.99747	0.72406	0.98204	0.98082	0.91793	0.73649	0.98249
T1_4	0.19837	0.96043	0.89367	0.99646	0.21411	0.95937	0.88809	0.99618
T1_5	0.38729	0.95464	0.81794	0.99308	0.74073	0.77236	0.91870	0.98677
T1_6	0.13697	0.96962	0.90521	0.99755	0.13539	0.97053	0.90347	0.99758
T1_7	0.33376	0.99868	0.95836	0.99404	1.94117	0.76615	0.79255	0.96534
T1_8	0.15901	0.97360	0.87385	0.99716	0.17003	0.97196	0.87279	0.99696
T2_1	0.05510	0.99480	0.97727	0.99902	0.04880	0.95121	0.97859	0.99913
T2_2	0.05353	0.99535	0.97542	0.99904	0.04723	0.94716	0.98080	0.99916
T2_3	0.07557	0.98251	0.97786	0.99865	0.07557	0.92457	0.97801	0.99865
T2_4	0.14799	0.98883	0.96996	0.99736	0.13539	0.89423	0.97112	0.99758
T2_5	0.28181	0.98424	0.96332	0.99497	0.40618	0.87790	0.92389	0.99275
T2_6	1.07685	0.99087	0.73777	0.98077	0.07557	0.94146	0.97212	0.99865
T2_7	0.08974	0.97363	0.97058	0.99840	0.07557	0.94146	0.97212	0.99865
T2_8	0.12910	0.98478	0.96234	0.99769	0.13539	0.92228	0.96169	0.99758

the original, known as the MSE value. Significantly better outcomes are obtained with significantly greater MSE. As a result, Peak-Signal-to-Noise-Ratio (PSNR) is one of the most widely-used quality indicators in reconstructing consistency. In other words, a more significant PSNR number indicates a better reconstruction. Calculate the error by squaring the difference between the predicted and actual values and averaging it across the dataset. MSE is also known as Quadratic loss, as the penalty is not proportional to the error but

Table 3
Quality performance analysis

Images	SOM K-Means							SOM-KFCM						
	Accuracy	Sensitivity	Specificity	Dice	Jacquard	MSE	PSNR	Accuracy	Sensitivity	Specificity	Dice	Jacquard	MSE	PSNR
Flair_1	0.861	0.843	0.866	0.764	0.882	0.319	53.124	0.986	0.995	0.304	0.180	0.545	0.098	58.274
Flair_2	0.597	0.597	0.748	0.597	0.988	17.435	35.751	0.869	0.871	0.225	0.126	0.430	0.202	55.106
Flair_3	0.908	0.986	0.845	0.731	0.882	1.280	47.093	0.875	0.999	0.072	0.037	0.671	0.038	62.313
Flair_4	0.914	0.994	0.826	0.703	0.893	1.843	45.510	0.717	0.996	0.044	0.023	0.715	0.041	61.996
Flair_5	0.922	0.986	0.820	0.694	0.908	1.565	46.219	0.760	0.967	0.091	0.047	0.758	0.053	60.957
Flair_6	0.909	0.905	0.786	0.647	0.910	0.867	48.784	0.781	0.999	0.164	0.090	0.776	0.048	61.318
Flair_7	0.899	0.970	0.839	0.722	0.873	2.669	43.901	0.742	0.996	0.427	0.271	0.714	0.076	59.331
Flair_8	0.291	0.122	0.210	0.117	0.856	4.468	41.664	0.953	0.928	0.788	0.650	0.956	0.093	58.465
T1_1	0.900	0.961	0.906	0.828	0.838	5.123	41.069	0.945	0.996	0.059	0.031	0.444	0.088	58.705
T1_2	0.860	0.892	0.861	0.756	0.830	5.824	40.513	0.515	0.972	0.133	0.071	0.497	0.132	56.964
T1_3	0.158	0.158	0.272	0.158	0.968	12.423	37.222	0.926	0.796	0.752	0.603	0.947	0.142	56.652
T1_4	0.876	0.845	0.854	0.746	0.899	5.260	40.955	0.935	0.996	0.237	0.135	0.613	0.081	59.083
T1_5	0.293	0.122	0.210	0.117	0.856	0.520	51.009	0.888	0.727	0.310	0.184	0.894	0.132	56.960
T1_6	0.898	0.893	0.837	0.720	0.900	5.533	40.736	0.878	0.988	0.259	0.149	0.703	0.055	60.765
T1_7	0.941	0.946	0.914	0.842	0.938	2.854	43.611	0.937	0.998	0.416	0.263	0.710	0.082	59.048
T1_8	0.800	0.860	0.833	0.714	0.719	5.498	40.763	0.850	0.996	0.194	0.107	0.411	0.078	59.226
T2_1	0.850	0.975	0.804	0.673	0.792	1.373	46.789	0.860	0.998	0.044	0.023	0.555	0.032	63.069
T2_2	0.926	0.955	0.873	0.775	0.915	1.621	46.066	0.991	0.928	0.056	0.029	0.688	0.028	63.764
T2_3	0.909	0.982	0.831	0.710	0.887	3.119	43.225	0.699	0.996	0.062	0.032	0.696	0.047	61.464
T2_4	0.913	0.994	0.825	0.702	0.893	0.482	51.331	0.724	0.972	0.089	0.047	0.720	0.039	62.268
T2_5	0.932	0.975	0.803	0.671	0.925	0.975	48.274	0.832	0.796	0.299	0.176	0.826	0.039	62.268
T2_6	0.888	0.889	0.775	0.633	0.888	0.461	51.524	0.713	0.999	0.084	0.044	0.709	0.043	61.816
T2_7	0.914	0.997	0.833	0.714	0.891	0.487	51.292	0.813	0.996	0.084	0.044	0.709	0.043	61.816
T2_8	0.916	0.997	0.830	0.710	0.895	0.467	51.474	0.930	0.928	0.118	0.063	0.725	0.047	61.478

Table 4
Performance evaluation of different MRI segmentation techniques

Techniques		Sensitivity	Accuracy	Specificity	Dice	Jacquard	MSE	PSNR	FOM
Proposed	SOM - Kmeans	0.827	0.913	0.758	0.644	0.884	3.436	45.329	0.77
	SOM-KFCM	0.951	0.974	0.221	0.143	0.684	0.073	60.129	0.319
Tarhini & Shbib (2020)	Threshold	0.852	0.888	0.768	-	-	-	-	-
	GLCM	0.721	0.814	0.667	-	-	-	-	-
	SVM	0.912	0.721	0.899	-	-	-	-	-
Sandhya et al. (2020)	CV model	85.868	0.849	82.65489	0.718	-	-	-	-
	SOM	89.96	0.908	89.68526	0.801	-	-	-	-
	FCM	87.86	0.864	84.85698	0.709	-	-	-	-
	PSO	89.86	0.898	87.08646	0.797	-	-	-	-
	ANN	90.96	0.916	91.31465	9.636	-	-	-	-
Sandhya et al. (2019)	SOM ACM	97.36	0.981	95.91567	0.877	-	-	-	-
	CV model	82.649	0.849	85.864	0.718	-	-	-	-
	SOM	89.68	0.908	91.454	0.801	-	-	-	-
	SOM ACM	95.91	0.981	97.358	0.877	-	-	-	-
Şişik & Eser (2020)	ELM-FRFCM	-	-	-	0.905505	0.841055	-	-	0.911115
	SVM	-	-	-	0.187975	0.15142	-	-	0.158715
	FCM	-	-	-	0.280995	0.176455	-	-	0.206845
	SOM	-	-	-	0.28124	0.17214	-	-	0.219145
Ejaz et al. (2020)	SOM K-means	-	-	-	0.988182	0.981818	0.04612	20.7352	
	SOM-FCM	-	-	-	0.973455	0.930636	0.2036	20.7464	
Asliyan & Atbakan (2020)	K-Means	-	0.93	-	-	-	-	-	-
	Fuzzy C-Means	-	0.92	-	-	-	-	-	-
	SOM	-	0.88	-	-	-	-	-	-
	Otsu	-	0.91	-	-	-	-	-	-
	K-Means+Otsu	-	0.94	-	-	-	-	-	-

to the square of the error. Squaring the error gives higher weight to the outliers, which results in a smooth gradient for small errors. Optimisation algorithms benefit from this penalisation for large errors as it helps find the optimum values for parameters. MSE will never be negative since the errors are squared.

Table 4 shows the comparison with state-of-the-art different MRI segmentation algorithms. The proposed segmentation techniques provide a higher Peak single-to-noise ratio, and it has a minimum mean square error. The overall accuracy of the proposed SOM-Kernal FCM techniques provides an accuracy of 95.1% when compared to the other deep learning-based segmentation techniques. Here we take different image quality analyses of different images and compare the proposed method results with the recent techniques. In addition, our proposed work considers more features and compares them with the state-of-the-art SOTA methods. These are explained in Table 4.

CONCLUSION

The proposed novel SOM-based KFCM technique for tumour segmentation identification was compared to other segmentation algorithms like K-means and FCM. The SOM-based KFCM segmentation method performs better than conventional methods, especially the SOM K-means method. The suggested method outperforms the KFCM and SOM-based KFCM techniques in PSNR. To summarise, the DOI value generated by the recommended approach is much greater than the traditional procedure. On the other hand, the proposed SOM-based KFCM method can identify tumours and segment tissues with high accuracy. Furthermore, the suggested methodology's operation may be improved, allowing it to segment noisy multimodal images.

ACKNOWLEDGEMENT

The authors thank the faculty members ECE department at the S.V. University College of Engineering, Tirupati, Andhra Pradesh, India, for their encouragement and cooperation.

REFERENCES

Al-Dmour, H., & Al-Ani, A. (2018). A clustering fusion technique for MR brain tissue segmentation. *Neurocomputing*, *275*, 546-559. https://doi.org/10.1016/j.neucom.2017.08.051

Anaraki, A. K., Ayati, M., & Kazemi, F. (2019). Magnetic resonance imaging-based brain tumor grades classification and grading via convolutional neural networks and genetic algorithms. *Biocybernetics and Biomedical Engineering*, *39*(1), 63-74. https://doi.org/10.1016/j.bbe.2018.10.004

Asliyan, R., & Atbakan, İ. (2020). Automatic brain tumor segmentation with K-means, fuzzy c-means, self-organizing map and otsu methods. *Selçuk-Teknik Dergisi*, *19*(4), 267-281.

Baalamurugan, K. M., Singh, P., & Ramalingam, V. (2021). A novel approach for brain tumor detection by self-organizing map (SOM) using adaptive network based fuzzy inference system (ANFIS) for robotic

systems. *International Journal of Intelligent Unmanned Systems, 10*(1), 98-116. https://doi.org/10.1108/IJIUS-08-2020-0038

Baid, U., Talbar, S., & Talbar, S. (2017). Comparative study of k-means, gaussian mixture model, fuzzy c-means algorithms for brain tumor segmentation. *Advances in Intelligent Systems Research*, *137*, 592-597.

Ejaz, K., Rahim, M. S. M., Bajwa, U. I., Chaudhry, H., Rehman, A., & Ejaz, F. (2020). Hybrid segmentation method with confidence region detection for tumor identification. *IEEE Access*, *9*, 35256-35278. https://doi.org/10.1109/ACCESS.2020.3016627

Garcia-Lamont, F., Cervantes, J., López, A., & Rodriguez, L. (2018). Segmentation of images by color features: A survey. *Neurocomputing, 292*, 1-27. https://doi.org/10.1016/j.neucom.2018.01.091

Guan, X., Yang, G., Ye, J., Yang, W., Xu, X., Jiang, W., & Lai, X. (2021). *3D AGSE-VNet: An automatic brain tumor MRI data segmentation framework*. ArXiv e-prints.

Helmy, A. K., & El-Taweel, G. S. (2016). Image segmentation scheme based on SOM–PCNN in frequency domain. *Applied Soft Computing, 40*, 405-415. https://doi.org.10.1016/j.asoc.2015.11.042

Huang, H., Yang, G., Zhang, W., Xu, X., Yang, W., Jiang, W., & Lai, X. (2021). A deep multi-task learning framework for brain tumor segmentation. *Frontiers in Oncology, 11*, Article 690244. https://doi.org/10.3389/fonc.2021.690244

Krishnakumar, S., & Manivannan, K. (2021). Effective segmentation and classification of brain tumor using rough K means algorithm and multi kernel SVM in MR images. *Journal of Ambient Intelligence and Humanized Computing*, *12*(6), 6751-6760.

Kumar, K. A., Kumar, B. M., Veeramuthu, A., & Mynavathi, V. S. (2019). Unsupervised machine learning for clustering the infected leaves based on the leaf-colors. In D. K. Mishra, X. S. Yang & A. Unal (Eds.), *Data Science and Big Data Analytics* (pp. 303-312). Springer.

Kumar, S. A., Harish, B. S., & Shivakumara, P. (2018). A novel fuzzy clustering based system for medical image segmentation. *International Journal of Computational Intelligence Studies, 7*(1), 33-66.

Mohan, G., & Subashini, M. M. (2018). MRI based medical image analysis: Survey on brain tumor grade classification. *Biomedical Signal Processing and Control*, *39*, 139-161.

Mohan, G., & Subashini, M. M. (2019). Medical imaging with intelligent systems: A review. In A. K. Sangaiah (Ed.), *Deep Learning and Parallel Computing Environment for Bioengineering Systems* (pp. 53-73). Academic Press.

Osman, A. H., & Alzahrani, A. A. (2018). New approach for automated epileptic disease diagnosis using an integrated self-organization map and radial basis function neural network algorithm. *IEEE Access*, *7*, 4741-4747.

Ren, T., Wang, H., Feng, H., Xu, C., Liu, G., & Ding, P. (2019). Study on the improved fuzzy clustering algorithm and its application in brain image segmentation. *Applied Soft Computing, 81*, Article 105503. https://doi.org/10.1016/j.asoc.2019.105503

Sandhya, G., Kande, G. B., & Satya, S. T. (2019). An efficient MRI brain tumor segmentation by the fusion of active contour model and self-organizing-map. *Journal of Biomimetics, Biomaterials and Biomedical Engineering, 40*, 79-91. https://doi.org/10.4028/www.scientific.net/JBBBE.40.79

Sandhya, G., Kande, G. B., & Savithri, T. S. (2020). Tumor segmentation by a self-organizing-map based active contour model (SOMACM) from the brain MRIs. *IETE Journal of Research*, 1-13. https://doi.org/10.1080/03772063.2020.1782780

Sheela, C., & Suganthi, G. J. M. T. (2020). Morphological edge detection and brain tumor segmentation in magnetic resonance (MR) images based on region growing and performance evaluation of modified fuzzy C-means (FCM) algorithm. *Multimedia Tools and Applications, 79*(25), 17483-17496. https://doi.org/10.1007/s11042-020-08636-9

Şişik, F., & Eser, S. E. R. T. (2020). Brain tumor segmentation approach based on the extreme learning machine and significantly fast and robust fuzzy C-means clustering algorithms running on Raspberry Pi hardware. *Medical Hypotheses*, *136*, Article 109507. https://doi.org/10.1016/j.mehy.2019.109507

Soltaninejad, M., Yang, G., Lambrou, T., Allinson, N., Jones, T. L., Barrick, T. R., Howe, F. A., & Ye, X. (2018). Supervised learning based multimodal MRI brain tumour segmentation using texture features from supervoxels. *Computer Methods and Programs in Biomedicine, 157*, 69-84. https://doi.org/10.1016/j.cmpb.2018.01.003

Song, Q., Wu, C., Tian, X., Song, Y., & Guo, X. (2022). A novel self-learning weighted fuzzy local information clustering algorithm integrating local and non-local spatial information for noise image segmentation. *Applied Intelligence, 52*(6), 6376-6397. https://doi.org/10.1007/s10489-021-02722-7

Tarhini, G. M., & Shbib, R. (2020). Detection of brain tumor in MRI images using watershed and threshold-based segmentation. *International Journal of Signal Processing Systems*, *8*(1), 19-25. https://doi.org/10.18178/ijsps.8.1.19-25

Vijh, S., Sharma, S., & Gaurav, P. (2020). Brain tumor segmentation using OTSU embedded adaptive particle swarm optimization method and convolutional neural network. In J. Hemanth, M. Bhatia & O. Geman (Eds.), *Data Visualization and Knowledge Engineering* (pp. 171-194). Springer. https://doi.org/10.1007/978-3-030-25797-2_8

Vishnuvarthanan, A., Rajasekaran, M. P., Govindaraj, V., Zhang, Y., & Thiyagarajan, A. (2017). An automated hybrid approach using clustering and nature inspired optimization technique for improved tumor and tissue segmentation in magnetic resonance brain images. *Applied Soft Computing*, *57*, 399-426. https://doi.org/10.1016/j.asoc.2017.04.023

Zhang, W., Yang, G., Huang, H., Yang, W., Xu, X., Liu, Y., & Lai, X. (2021). ME-Net: multi-encoder net framework for brain tumor segmentation. *International Journal of Imaging Systems and Technology, 31*(4), 1834-1848. https://doi.org/10.1002/ima.22571

Zhang, Z., & Sejdić, E. (2019). Radiological images and machine learning: Trends, perspectives, and prospects. *Computers in Biology and Medicine*, *108*, 354-370. https://doi.org/10.1016/j.compbiomed.2019.02.017